# **Inorganic Chemistry**

pubs.acs.org/IC Article

# Silver 2,4'-Bipyridine Coordination Polymer for the High-Capacity Trapping of Perrhenate, A Pertechnetate Surrogate

Beatriz Ehlke, Cambell S. Conour, Tyler J. Vandiver, Kevin C. Lofgren, Jeremy L. Barnett, Eric W. Reinheimer, John S. Wenger, and Scott R. J. Oliver\*



**ACCESS** I

Cite This: Inorg. Chem. 2024, 63, 8674-8684



Article Recommendations

Metrics & More  $ReO_{4^{-}(aq)}$ 

ABSTRACT: Pertechnetate, the most stable form of the radionuclide 99Tc in aerobic aqueous systems, is a hazardous anion present in nuclear waste. Its high mobility in water makes the remediation of the anion challenging. In the past decade, significant effort has been placed into finding materials capable of adsorbing this species. Here, we present the synthesis and high-resolution crystal structure of the coordination polymer [Ag(2,4'-bipyridine)]NO<sub>3</sub>, which is capable of sequestering perrhenate—a pertechnetate surrogate—through anion exchange to form another new coordination polymer, [Ag(2,4'-bipyridine)]ReO<sub>4</sub>. Both the beginning and end structures were solved by single-crystal X-ray diffraction and the adsorption reaction was monitored through inductively coupled plasma-optical emission spectroscopy and UV-vis spectroscopy. The exchange reaction follows a pseudo-second-order mechanism and the maximum adsorption capacity is 764 mg ReO<sub>4</sub>/g [Ag(2,4'-bipyridine)]NO<sub>3</sub>, one of the highest recorded for a coordination polymer or metal-organic framework. A solvent-mediated recrystallization mechanism was determined by monitoring the ionexchange reaction by scanning electron microscopy—energy-dispersive spectroscopy and powder X-ray diffraction.

# INTRODUCTION

Technetium is a hazardous radionuclide introduced into nature mainly by anthropological sources and it is estimated that 1 kg of the radionuclide is produced for every ton of enriched uranium fuel fissioned. Once in aqueous systems, the most stable form of the long-lived 99Tc is the pertechnetate ion TcO<sub>4</sub>-, with high water mobility due to its high solubility and weak coordination. Currently, one of the most common strategies for the remediation of pertechnetate focuses on the use of sorption methods using the anion itself or perrhenate as a less hazardous surrogate. Recent studies employ bentonites, carbazole derivatives, acationic electrospun fibers, modified commercial works, <sup>9-11</sup> mineral incorporation, <sup>12</sup> and coordination polymers (CPs). <sup>13-16</sup>

Among these options, CPs are promising for adsorption applications because they are versatile materials that can be tailored in terms of structural features that are fundamental for successful ion exchange, namely framework charge, topology, and pore size. These polymeric materials are composed of metal centers connected by organic linkers and may possess variable covalent dimensionality. More specifically, cationic CPs - obtained by using low-valence cationic metals and neutral ligands - are of particular interest for anion exchange applications, <sup>17–19</sup> as they possess weakly bound counter-anions. For example, MOR-2 is a zinc-based material obtained by Rapti et al. and presents an adsorption capacity of 876 mg/g (mg ReO<sub>4</sub> per gram of material), the current record for this class of materials. 13 Our group previously reported [Ag(pyrazine)] NO<sub>3</sub>, a cationic CP with uptake capacity of 818 mg/g. <sup>17</sup> Wang et al. have studied a variety of cationic CPs presenting high perrhenate uptake, such as SBN (786 mg/g).<sup>20</sup> The Wang group has also reported SCU-100, a polymeric material based on silver and nitrogen-donating ligands that not only presented a high uptake of 541 mg/g but also performed well when using pertechnetate itself instead of perrhenate, reaching 87% TcO<sub>4</sub><sup>-</sup> removal.<sup>21</sup>

Supporting Information

Received: January 16, 2024 April 7, 2024 Revised: Accepted: April 22, 2024 Published: May 1, 2024





Two main mechanisms by which CP's undergo ion-exchange reactions have been proposed: single-crystal to single-crystal (SCSC) transition and solvent-mediated recrystallization. Mechanistic elucidation can be achieved by combining a variety of crystal diffraction and microscopy techniques, which allow for the observation of phase transitions as well as morphological distortions and ion diffusion behavior. Shao et al. have detailed a SC-SC mechanism occurring for the trapping of HCrO<sub>4</sub><sup>-</sup> in a copper-based coordination polymer. Their study revealed that the morphology and size features of the original crystal did not change during the exchange reaction. In addition, similar crystallographic parameters for the pre- and postexchange materials were observed.<sup>22</sup> Conversely, recrystallization usually involves more substantial crystallinity changes. In the case of one-dimensional (1D) CPs composed of Ag(I) and 4,4'bipyridine, Schröder et al. demonstrated that anion-exchange reactions undergo a recrystallization pathway through a selfperpetuating cascade. Microscopy studies on the uptake of  $NO_3^-$  ions by the coordination polymer [Ag(4,4'-bipyridine)]-BF<sub>4</sub> revealed that the crystal surface of the initial material was significantly modified during the ion-exchange reaction.<sup>23,24</sup>

Here, we report a cationic coordination polymer  $[Ag(2,4'-bipyridine)]NO_3$  (which we denote SLUG-53, for the University of California, Santa Cruz, Structure No. 53) and its ability to sequester perrhenate via a solvent-mediated recrystallization reaction to form  $\{[Ag(2,4'-bipyridine)]ReO_4, which we denote SLUG-54\}.$ 

# **■ EXPERIMENTAL SECTION**

**Materials.** All reagents were used as-purchased: silver nitrate (Thermo Scientific, 99.9+%), 2,4'-bipyridine (2,4'-bipy, TCI), sodium perrhenate (Alfa Aesar, 99.95%), and sodium sulfate anhydrous (Fisher Scientific).

**Synthesis of [Ag(2,4'-bipy)]NO**<sub>3</sub> (**SLUG-53).** Five mL aqueous solution of AgNO<sub>3</sub> (4.000 mmol, 0.6795 g) was added dropwise to 5 mL aqueous solution of 2,4'-bipyridine (1.000 mmol, 0.1562 g) under magnetic stirring. Upon addition, a white solid instantly precipitated. The resultant suspension was transferred to a Teflon-lined stainless-steel autoclave, placed in an oven at 145 °C for 5 d, and then slowly cooled to room temperature at a rate of 0.1 °C/min. Colorless needle crystals suitable for single-crystal X-ray diffraction (SCXRD) were isolated by vacuum filtration and rinsed with Milli-Q water. Yield based on 2,4'-bipyridine: 76.7%. A polymorph of SLUG-53 has been reported in the literature and will be discussed below. That material was synthesized by combining methanolic equimolar solutions of AgNO<sub>3</sub> and 2,4'-bipyridine at 50 °C. <sup>25</sup>

Synthesis of [Ag(2,4'-bipy)]ReO<sub>4</sub> (SLUG-54). An anion exchange reaction between SLUG-53 and NaReO<sub>4</sub> was prepared by placing 0.200 mmol (0.0652 g) of SLUG-53 in a beaker containing 10 mL of Milli-Q water and NaReO<sub>4</sub> (0.200 mmol, 0.0546 g), resulting in a white powder. Yield based on NaReO<sub>4</sub>: 69.5%. For large single crystals, an identical reaction mixture was transferred to a Teflon-lined stainless-steel autoclave, kept at 145 °C for 3 days, and then slowly cooled to room temperature at a 0.1 °C/min rate. Colorless needle crystals suitable for SCXRD were isolated by vacuum filtration and rinsed with Milli-Q water. Yield based on NaReO<sub>4</sub>: 43.3%.

**Perrhenate Uptake Quantification.** Adsorption kinetics were studied by performing an exchange reaction between SLUG-53 and NaReO<sub>4</sub> as described above. Aliquots were collected at 5 min, 30 min, 1 h, 2 h, 3 h, 4 h, 8 h, 16 h, 24 h, 32 h, 40 h, 48 h, and 72 h, syringe filtered and then analyzed by ICP-OES. The data was fitted to a pseudo-second-order model described in eq 1.

$$\frac{t}{q_{t}} = \frac{1}{k_{2}q_{e}^{2}} + \frac{t}{q_{e}} \tag{1}$$

where t is the reaction time (min),  $q_t$  is the material's adsorption at time t (mg·g<sup>-1</sup>),  $k_2$  is the rate constant (g·mg<sup>-1</sup>·min<sup>-1</sup>), and  $q_e$  is the adsorption capacity at equilibrium (mg·g<sup>-1</sup>).

Sorption isotherms were obtained by placing 10 mg of CP in contact with 10 mL solutions of NaReO $_4$  with concentrations varying from 100 to 1000 ppm. The reactions were kept under magnetic stirring for 24 h. Aliquots were collected for each reaction, syringe filtered, and then analyzed by ICP-OES. The data was fitted to a Langmuir model as described in eq 2.

$$\frac{C_{\rm e}}{q_{\rm e}} = \frac{1}{q_{\rm m}K_{\rm L}} + \frac{C_{\rm e}}{q_{\rm m}} \tag{2}$$

where  $C_{\rm e}$  is the concentration of perrhenate ions at equilibrium (mg·L<sup>-1</sup>),  $q_{\rm m}$  is the maximum adsorption capacity (mg·g<sup>-1</sup>), and  $K_{\rm L}$  is the Langmuir model constant (L·mg<sup>-1</sup>). Both the adsorption kinetics and isotherms were obtained in triplicate.

**Selectivity Studies.** SLU $\overline{G}$ -53 selectivity to uptake perrhenate was studied under two different molar excesses of sulfate. For a 50-fold excess, 0.4000 mmol (0.1304 g) of SLU $\overline{G}$ -53 was placed in a beaker containing 20 mL of Milli-Q water, NaReO<sub>4</sub> (0.4000 mmol, 0.1093 g), and Na<sub>2</sub>SO<sub>4</sub> (20.000 mmol, 2.8408 g). For a 200-fold excess, 0.4000 mmol (0.1304 g) of SLU $\overline{G}$ -53 was placed in a beaker containing 50 mL of Milli-Q water, NaReO<sub>4</sub> (0.4000 mmol, 0.1093 g), and Na<sub>2</sub>SO<sub>4</sub> (80.0000 mmol, 11.3632 g). A higher volume of water was used for the 200-fold excess reaction to guarantee the dissolution of the sulfate salt. Both reactions were performed in triplicate, syringe filtered, and the filtrate was analyzed by ICP-OES for elemental quantification.

A similar experiment was conducted but with nitrate instead of sulfate ions. For a 50-fold excess, 0.4000 mmol (0.1304 g) of SLUG-53 was placed in a beaker containing 20 mL of Milli-Q water, NaReO<sub>4</sub> (0.4000 mmol, 0.1093 g), and NaNO<sub>3</sub> (20.000 mmol, 1.6998 g). For a 200-fold excess, 0.4000 mmol (0.1304 g) of SLUG-53 was placed in a beaker containing 20 mL of Milli-Q water, NaReO<sub>4</sub> (0.4000 mmol, 0.1093 g), and NaNO<sub>3</sub> (80.0000 mmol, 6.7992 g). Both reactions were performed in triplicate, syringe filtered, and the filtrate was analyzed by ICP-OES for elemental quantification.

**Elemental Analysis.** The concentrations of Re and Ag in the samples were obtained by ICP-OES on a PerkinElmer Optima 4300DV using yttrium as an internal standard and rhenium and silver solutions as external standards. The Re concentrations were then converted to perrhenate to be used in the kinetics and adsorption model studies. The equipment detection limits for Re and Ag were 5 and 3 ppb, respectively.

Thermal Stability Analysis. Thermogravimetric analyses (TGA) were performed under nitrogen flow on a TA Instruments Q500 TGA with a temperature range of 25-500 °C at a heating rate of 10 °C/min.

**Powder X-ray Diffraction (PXRD).** PXRD samples were prepared by grinding the synthetic products with a mortar and pestle and placing the resulting materials in an aluminum sample holder. The data was collected on a Rigaku Americas Miniflex Plus powder diffractometer under Cu K $\alpha$  radiation ( $\lambda$  = 1.5418 Å) with a scanning range of 2–35° (2 $\theta$ ) at a rate of 2°/min with a 0.02° step size.

**Variable Temperature PXRD (VT-PXRD) Analysis.** Ex situ variable temperature PXRD (VT-PXRD) was performed by heating the samples in a box furnace oven to 100, 200, 275, 300, 400, and 500 °C at a rate of 2°/min in air. The samples were analyzed on a Rigaku SmartLab X-ray Diffractometer with Cu K $\alpha$  radiation ( $\lambda$  = 1.5418 Å) in parallel beam geometry from 2–50° ( $2\theta$ ) at a scan rate of 2°/min and 0.02° step size.

Single-Crystal X-ray Diffraction (SCXRD). Colorless crystals having dimensions  $0.43 \times 0.11 \times 0.06 \text{ mm}^3$  (SLUG-53-RT\*),  $0.50 \times 0.06 \times 0.05 \text{ mm}^3$  (SLUG-53),  $0.20 \times 0.17 \times 0.13 \text{ mm}^3$  (SLUG-54), and  $0.11 \times 0.08 \times 0.05 \text{ mm}^3$  (SLUG-54-RT\*), were secured to Mitegen micromounts using Paratone oil. Their SCXRD data was collected using a Rigaku Oxford Diffraction (ROD) Synergy-S X-ray diffractometer equipped with a HyPix-6000HE hybrid photon counting (HPC) detector and microfocused Cu K $_{\alpha 1}$  radiation ( $\lambda$  = 1.54184 Å). All data were collected at 100 K except for SLUG-53-RT and SLUG-54-RT, whose data was collected at 287 and 298 K, respectively. Data

collection strategies for all samples to ensure completeness and desired redundancy were determined using CrysAlis<sup>Pro</sup>. <sup>26</sup> Data processing was performed using CrysAlis<sup>Pro</sup> and included numerical absorption corrections determined via face-indexing for samples SLUG-53-RT, SLUG-54, and SLUG-54-RT. A multiscan absorption correction was applied to SLUG-53 using the SCALE3 ABSPACK scaling algorithm. All structures were solved via intrinsic phasing methods using ShelXT<sup>28</sup> and refined using ShelXL<sup>29</sup> in the Olex2 graphical user interface.<sup>30</sup> Space groups were unambiguously verified by PLATON.<sup>31</sup> The final structural refinement included anisotropic temperature factors on all non-hydrogen atoms. All hydrogen atoms were attached via the riding model at calculated positions using suitable HFIX commands. Selected crystallographic parameters are given in Tables S1 and S2. Optical micrographs of SLUG-53 and SLUG-54 morphologies are depicted in Figure S1. Thermal ellipsoid plots for SLUG-53, SLUG-53-RT, SLUG-54, and SLUG-54-RT are shown in Figures S2-S5, respectively.

\*SLUG-53-RT and SLUG-54-RT materials were synthesized as described in the Experimental Section but with SCXRD data collected at room temperature.

Scanning Electron Microscopy-Energy Dispersive X-ray Spectroscopy (SEM-EDS). SLUG-53 single crystals (0.6100 mmol, 0.2000 g) were submerged in a 30 mL aqueous solution containing sodium perrhenate (0.6100 mmol, 0.1672 g). Crystals were collected at 1 min, 4, and 72 h. The SLUG-53 initial material and the collected crystals were mapped for Re in a Thermo Scientific Apreo scanning electron microscope coupled with an energy-dispersive X-ray spectrometer operating at 18.00 kV and 0.50 nA.

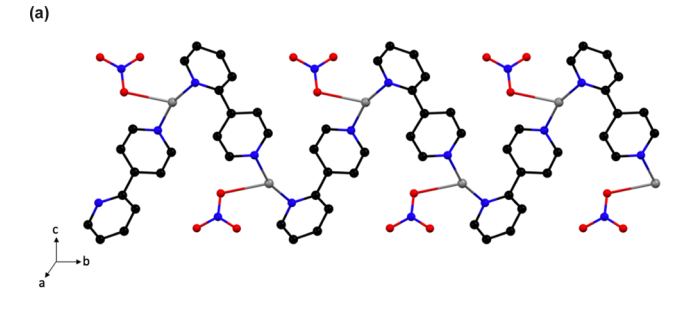
UV-Vis Analysis. UV-Vis analysis was performed using quartz cuvettes on a Hewlett-Packard model 8452A UV-vis spectrophotometer with wavelength ranging from 190 to 820 nm.

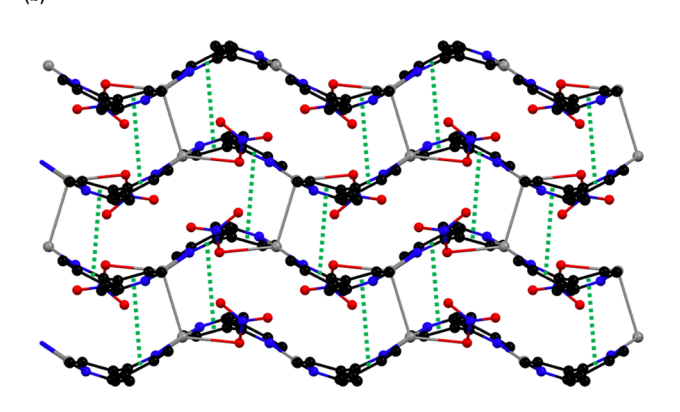
**Optical Microscopy.** The morphologies of SLUG-53 and SLUG-54 crystals were examined on a Zeiss Axioskop 2 MAT microscope under bright-field light and 5× augmentation lens.

# ■ RESULTS AND DISCUSSION

[Ag(2,4'-bipy)]NO<sub>3</sub> (SLUG-53) was synthesized by the combination of the organic ligand 2,4'-bipyridine and silver nitrate. The low coordination number and +1 oxidation state of silver coupled with the neutral ligand allowed the formation of a coordination polymer with the cationic stoichiometry [Ag(2,4'-bipy)<sup>+</sup>], counterbalanced by nitrate ions from the silver salt reagent. In order to guarantee an extended polymeric structure, a molar excess of silver nitrate in relation to 2,4'-bipy was necessary. Equimolar reactions led to the formation of a molecular solid (SLUG-55), as confirmed by SCXRD. Although showing significant disorder in the solvent molecules and nitrate groups, the structure was confirmed to have nonpolymeric connectivity (Figure S6). A molar excess of AgNO<sub>3</sub> as low as 1.5 times and as high as 4 times resulted in phase-pure SLUG-53 (Figure S7).

Structural Description of SLUG-53. SLUG-53 crystallizes in space group  $P2_1/c$  as colorless needle crystals. Its structure consists of zigzag chains growing in the direction of the crystallographic b-axis, formed by covalent bonds between silver and the nitrogen atoms of the 2,4'-bipy (Figure 1a). Each silver atom connects to two ligands, binding through the nitrogen in the 4' position of one 2,4'-bipy (N2) and the 2 position of a second 2,4'-bipy (N3). Each ligand binds to another silver atom through its second nitrogen, leading to the modulating polymer. The Ag-N3 bond length is 2.203(4) Å and the Ag-N2 bond length is 2.179(3) Å. The silver also binds to one oxygen of a nitrate ion, with an Ag-O3 distance of 2.590(3) Å. The zigzag chains are not perfectly flat, with an N2-Ag-N3 angle of 163.73(13)°, resulting in a distorted T-shape geometry for the silver centers. The nitrate ions are positioned in the pockets of the zigzags, with only one of its oxygen atoms (O3) interacting





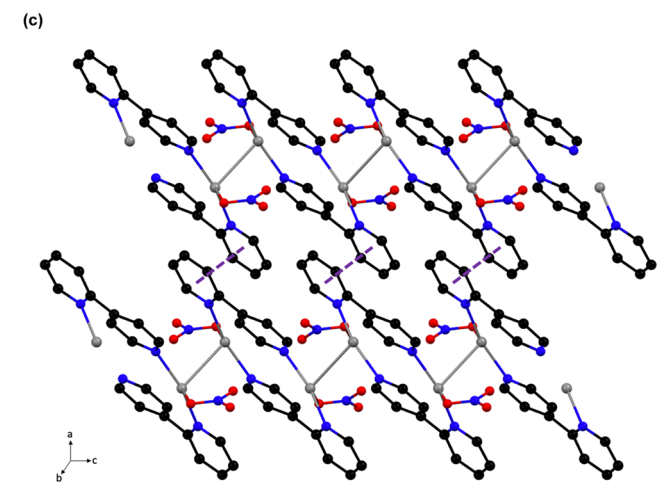


**Figure 1.** Crystal structure of SLUG-53 obtained by SCXRD at 100 K: (a) projection along the *a*-axis, showing one polymeric zigzag chain formed by alternating Ag and 2,4′-bipy units. Nitrate anions reside in the pockets of the chain; (b) view parallel to the crystallographic (102) plane, showing the stacking of zigzag chains through both argentophilic interactions (solid gray lines), and  $\pi$ -stacking (dashed green lines); (c) *b*-projection, the layers described in panel (b) interact with each other through additional  $\pi$ -stacking, here showed by dashed purple lines. Hydrogen atoms omitted for clarity; color scheme: Ag – light gray; N – blue; O – red; and C – black.

with the silver. Therefore, the nitrates do not participate in extending the 1D zigzag chains into a two-dimensional (2D) layer or three-dimensional (3D) framework. Instead, the zigzag chains form a secondary structure by stacking upon each other through argentophilic interactions (Figure 1b). Such interactions are generally accepted to occur whenever silver atoms with electronic configuration [Kr]d<sup>10</sup> are at a distance smaller than 3.44 Å—twice the van der Waals radius of Ag—in a crystal

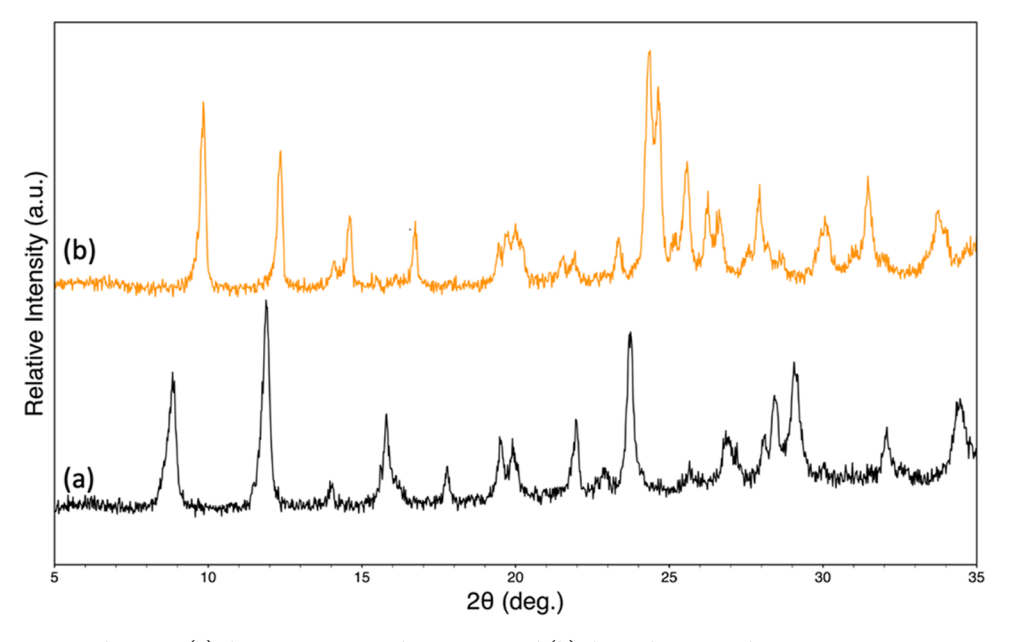
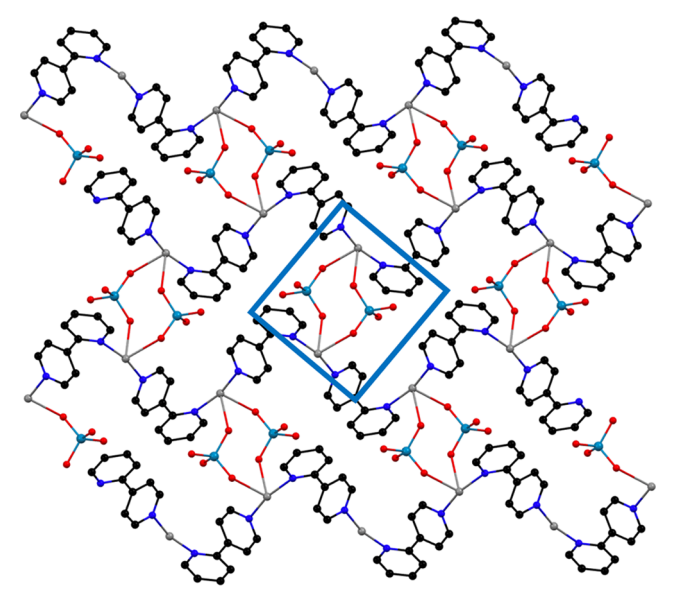


Figure 2. PXRD comparison between (a) the starting material SLUG-53 and (b) the exchange product SLUG-54.



**Figure 3.** Crystal structure of SLUG-54 obtained by SCXRD at 100 K. Zigzag chains similar to SLUG-53 are again observed. The counteranion, however, now has a fundamental role in extending the structure through the formation of eight-membered rings containing silver atoms (emphasized as a blue rectangle). Color scheme: Ag - light gray; N - blue; O - red; and Re - light blue. All hydrogens are omitted for clarity.

lattice. <sup>32</sup> Due to the asymmetry of the ligand and in order to maximize the argentophilic interactions, the zigzag chains are not perfectly parallel to each other but slightly shifted to allow closer contact between the silver centers. Further, neighboring zigzag chains are of opposite handedness and allow for a shorter Ag–Ag distance of 2.9949(6) Å. In addition to the argentophilic interactions, there is also interchain  $\pi$ -stacking of the 2,4′-bipy rings (green dashed lines, Figure 1b). Because of the opposite handedness, this  $\pi$ -stacking occurs between the N2 and N3 rings, which are separated by 3.685(3) Å. Finally, a second  $\pi$ -stacking interaction connects the stacked zigzag layers, resulting in the overall 3D structure (purple dashed lines, Figure 1c). This interaction occurs between two N3 rings, each ring belonging to

a different set of layered zigzag chains with a distance of 3.749(4) Å.

A polymorphic CP of SLUG-53 crystallizes in the *Pbca* space group and has been reported in the literature.<sup>25</sup> In that compound, the silver atoms still bind to two nitrogens from the ligands and one oxygen from NO<sub>3</sub><sup>-</sup>, resulting in a distorted T-shape geometry. The zigzag chains of alternating Ag and 2,4′-bipy are again observed; however, the fashion in which they are arranged differs as they are no longer shifted toward each other to maximize argentophilic interactions. As a result, the Ag–Ag distance is increased to 3.9868(5) Å, outside the covalent range. Further crystallographic comparison is given in Table S3.

In order to determine if the single crystal collected for SCXRD was representative of the bulk sample, we compared the theoretical powder pattern calculated from the single crystal data to that obtained experimentally by PXRD of the SLUG-53 needle crystals. Observing Bragg's Law, slight  $2\theta$  angle shifts are expected when comparing calculated versus theoretical patterns since PXRD and SCXRD data were collected at different temperatures (287 and 100 K, respectively). Usually, there is a shrinking of the unit cell at lower temperatures and, consequently, the diffraction planes are closer together. However, a significant mismatch of diffraction peaks was noticed when we compared the theoretical and experimental patterns for SLUG-53 (Figure S8). Because of that, a new SCXRD analysis on a different crystal was performed at room temperature.

The room temperature SCXRD analysis revealed an anisotropic thermal distortion of the unit cell. Rather than uniformly shrinking at lower temperatures, an overall deformation occurred with the crystallographic *a*-axis decreasing by 7%, the crystallographic *b*-axis decreasing by 0.6% and the crystallographic *c*-axis *increasing* by 5%. Although unusual, particularly the increase of the unit cell along the *c*-axis, these distortions correlate well with the chemical structure of SLUG-53. The polymeric chain possesses stronger Ag–N covalent bonds in the *b* direction, while in the *a* and *c* directions are weaker van der Waals interactions. As a result, the latter two axes would be more susceptible to temperature-related distortions. Neither SLUG-53 nor SLUG-53-RT showed inter- or intra-

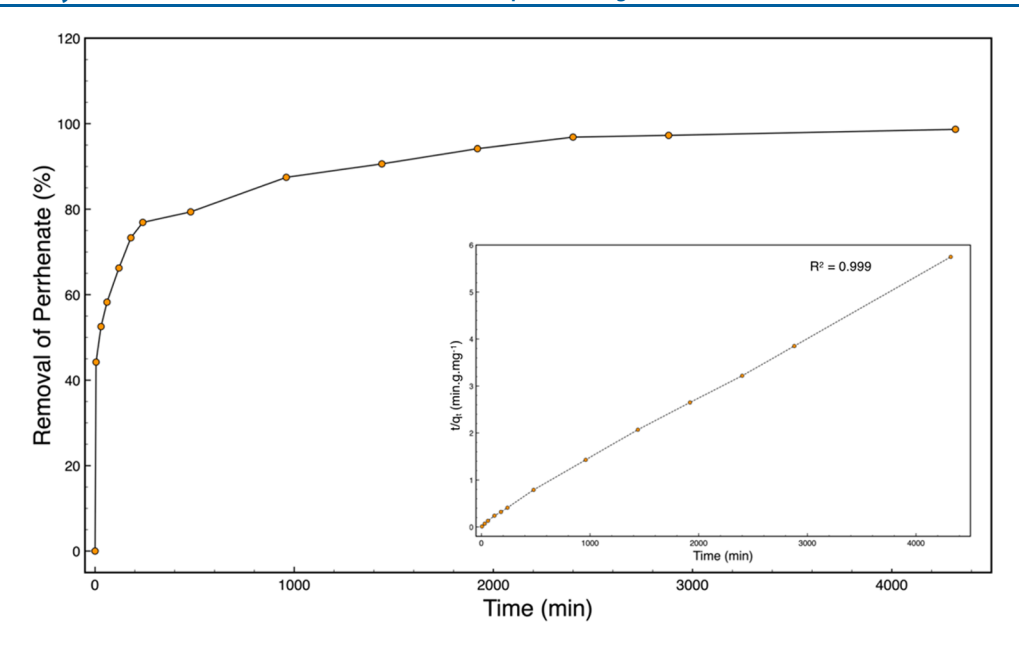


**Figure 4.** Percentage of perrhenate removed by SLUG-53 as a function of time. Data points were obtained for SLUG-53/perrhenate solution contact times of 5 min, 30 min, 1 h, 2 h, 3 h, 4 h, 8 h, 16 h, 24 h, 32 h, 40 h, 48h, and 72 h. Starting  $ReO_4^-$  solution: 0.01994 mol/L and final  $ReO_4^-$  solution after 72 h: 0.00046 mol/L. pH of initial perrhenate solution = 6.98. pH immediately after the SLUG-53 addition = 6.30. pH at 72 h = 6.68 (inset: data fitting to pseudo-second-order model).

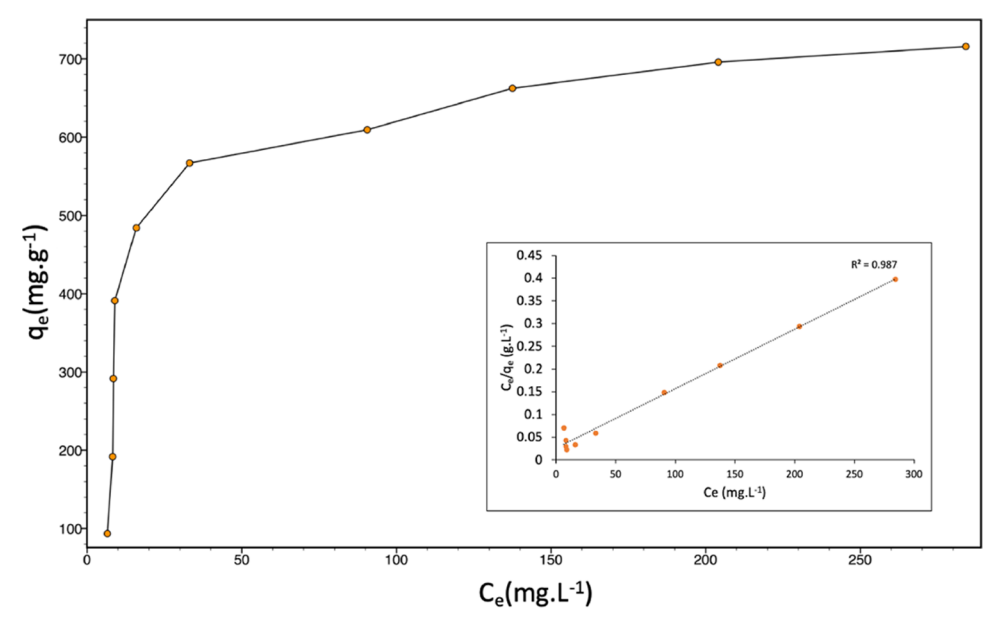


Figure 5. Adsorption capacity of SLUG-53 as a function of equilibrium concentration (inset: data fitting to Langmuir model).

molecular hydrogen bonds (as calculated in Mercury<sup>33</sup>). Selected structural parameters are displayed in Table S4. The structure overlay of SLUG-53 and SLUG-53-RT is depicted in Figure S9.

Anion Exchange with ReO<sub>4</sub><sup>-</sup>. The novel CP SLUG-53 successfully exchanges its loosely bound nitrate for perrhenate (surrogate for the hazardous pertechnetate). The powder pattern of the exchange product is very similar to that of SLUG-53, but there is an important shift of the earlier peaks to higher angles (Figure 2). The similarity between the patterns suggests the covalent framework is preserved, while the shifts indicate that the new framework is likely wrapping around the incoming perrhenate ions. To strengthen this theory, we were able to recrystallize the exchange product and solve the

compound as [Ag(2,4'-bipy)]ReO<sub>4</sub> (SLUG-54). The initial exchange product and the recrystallized material presented the same PXRD pattern, confirming that no phase change was observed after hydrothermal treatment.

**Structural Description of SLUG-54.** The structure of SLUG-54 is presented in Figure 3. It also consists of polymeric zigzag chains built by the alternation of silver and 2,4'-bipyridine units in a similar fashion to SLUG-53, as expected by the powder pattern. The Ag-N1 distance is 2.202(5) Å and Ag-N2 is 2.183(5) Å (N1 and N2 being the 2 and 4' nitrogens of 2,4'-bipy, respectively). Once again, the chains are not perfectly planar, with an N1-Ag-N2 angle of 165.9(2)°. The main difference between the two CPs is the role of the counteranion in building the overall structure. In SLUG-53, the nitrate ions

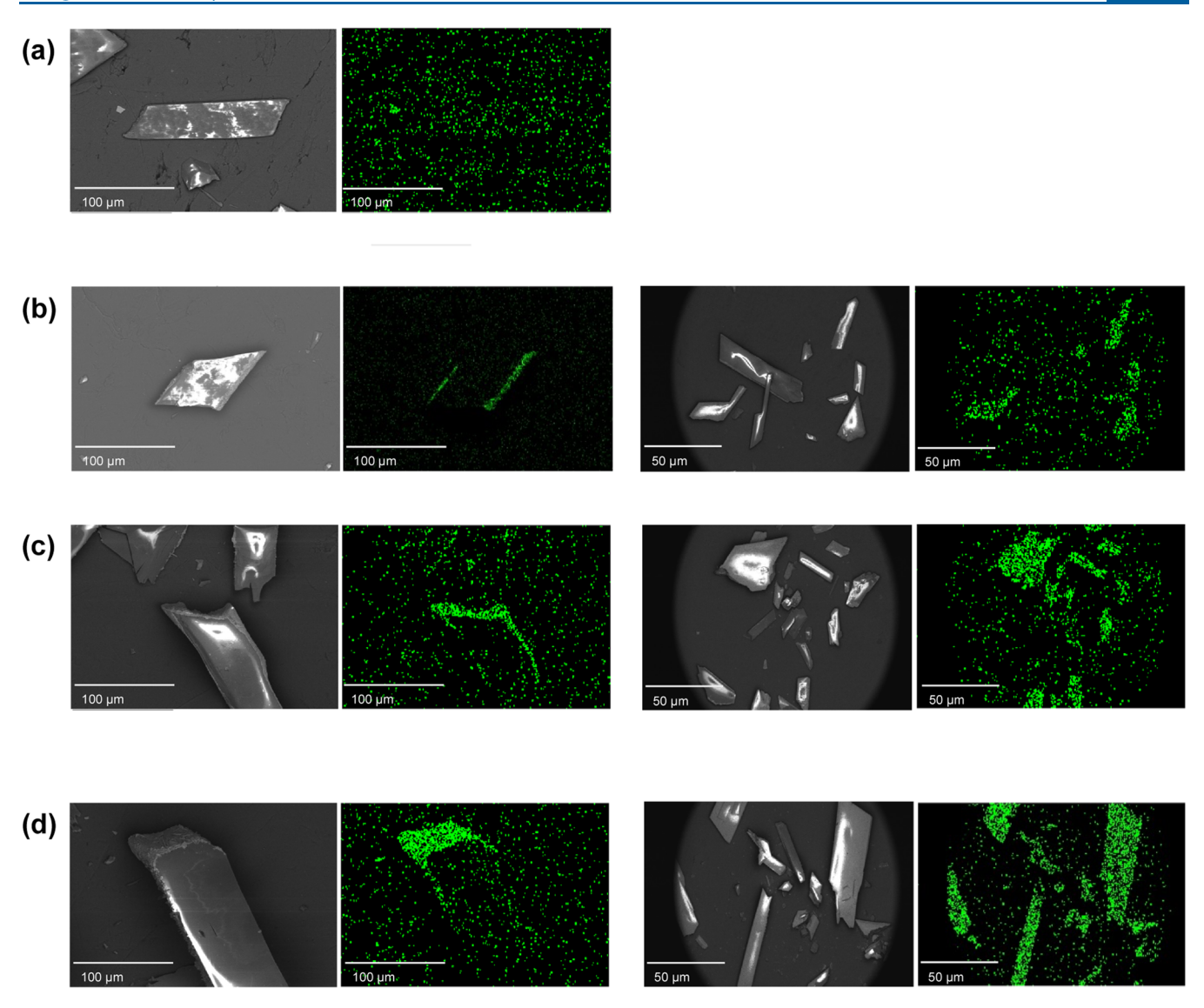


**Figure 6.** SEM images and EDS mapping of Re (green) of anion exchange reactions' products. SLUG-53 single crystals were used as starting material. Reaction times: (a) t = 0 min; (b) t = 1 min; (c) t = 4 h; and (d) 72 h. The bright areas in the SEM images are due to the charging intrinsic of the material.

reside in the zigzag pockets and interact with only one silver atom. In SLUG-54, the perrhenate ions are the primary units responsible for connecting adjacent chains. Due to its much larger size, perrhenate ions do not fit in the zigzag pockets the same way the nitrate ions do. The rhenium atom resides in the same plane as the zigzag chains, while the oxygen atoms reside in the interchain spacing. An eight-membered ring is thereby formed by two ReO<sub>4</sub> units bridging two silver atoms from adjacent zigzag chains, with bond lengths Re-O1 = 1.733(4) Å, Re-O4 = 1.730(5) Å, Ag-O4 = 2.617(5) Å and Ag-O1 =2.588(5) Å. The other two oxygens of the perrhenate ion, O2 and O3, do not covalently interact with another atom. No argentophilic interactions are present, with the closest Ag atoms standing at 4.2693(8) Å apart. The thermal flexibility of SLUG-54 was also investigated to determine if an anisotropic distortion similarly to the one observed for SLUG-53 was present. The room temperature single-crystal analysis did not reveal major variations in the unit cell axis (Table S2), as expected due to the greater degree of covalent connectivity and the similarity between the powder patterns. Similar to the SLUG-53 structures, neither intra- nor intermolecular hydrogen bonds were observed in Mercury.<sup>33</sup> The structural overlay of SLUG-53 and SLUG-54 is depicted in Figure S10.

**ReO**<sub>4</sub><sup>-</sup> **Exchange Quantification.** To better understand the dynamics of the conversion of SLUG-53 to SLUG-54, we investigated the exchange reactions over different periods of time. The UV-vis analysis of the filtrates of these reactions revealed the increase of the nitrate peak intensity, indicating the release of this species upon the adsorption of perrhenate (Figure S11). ICP-OES was used to quantify the perrhenate uptake. The percentage removals and adsorption capacities for the reactions at different times are given in Table S5. Figure 4 and Table S6 show that the data fits well as a pseudo-second-order reaction. The data was also tested as a pseudo-first-order reaction but showed significantly poorer fitting ( $R^2 = 0.761$ ).

To determine the maximum adsorption capacity, sorption isotherms were obtained by adding 10 mg of SLUG-53 to 10 mL of perrhenate solution with concentrations varying from 100 to 1000 ppm. All reactions were kept under stirring for 24 h to guarantee equilibrium was reached. The data fit well with the

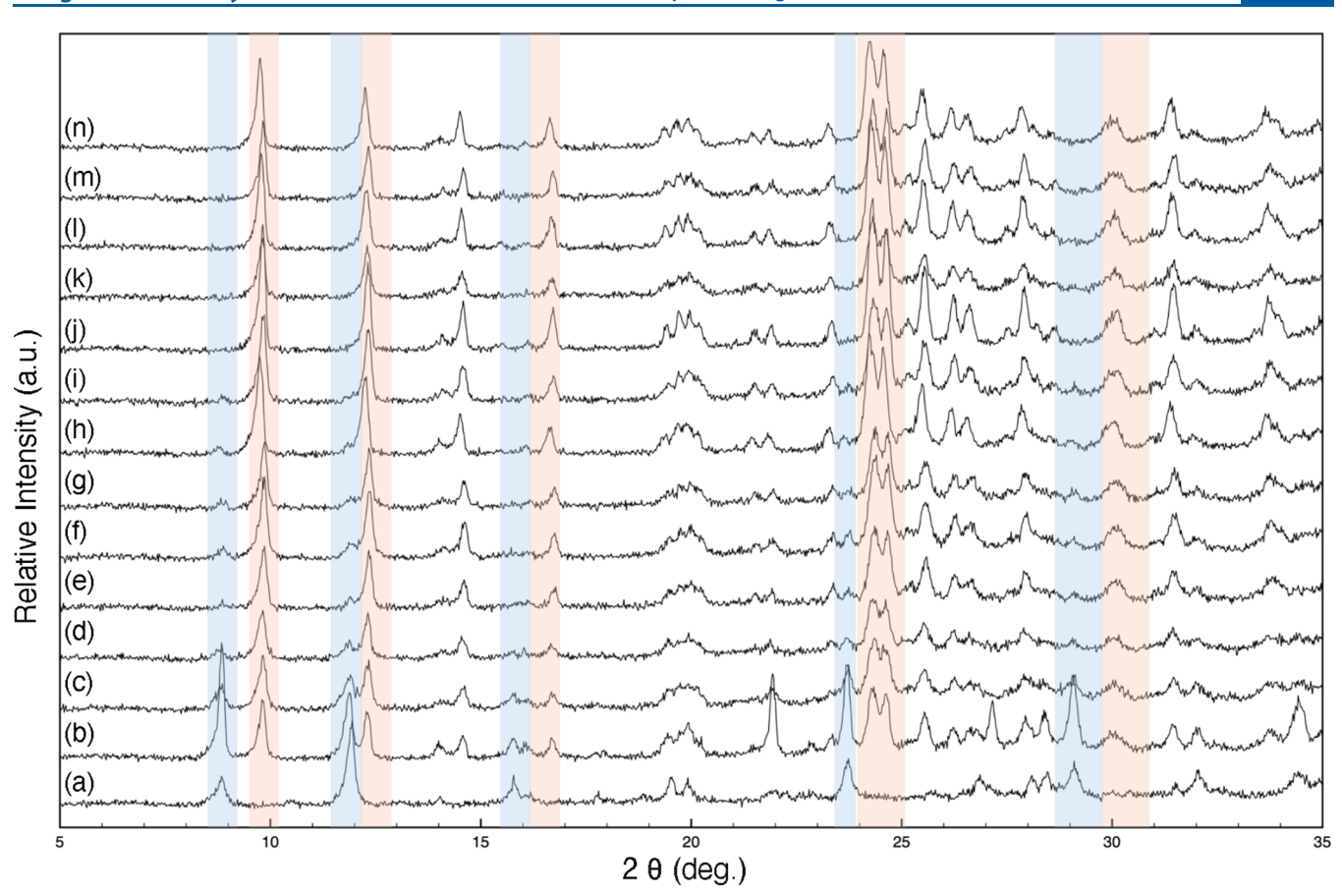


Figure 7. Monitoring of the anion exchange reaction by PXRD. Reaction lengths: (a) 0 min (b) 5 min; (c) 30 min; (d) 1 h; (e) 2 h; (f) 3 h; (g) 4 h; (h) 8 h; (i) 16 h; (j) 24 h; (k) 32 h; (l) 40 h; (m) 48 h; and (n) 72 h. Characteristic peaks of SLUG-53 and SLUG-54 are highlighted in blue and orange, respectively.

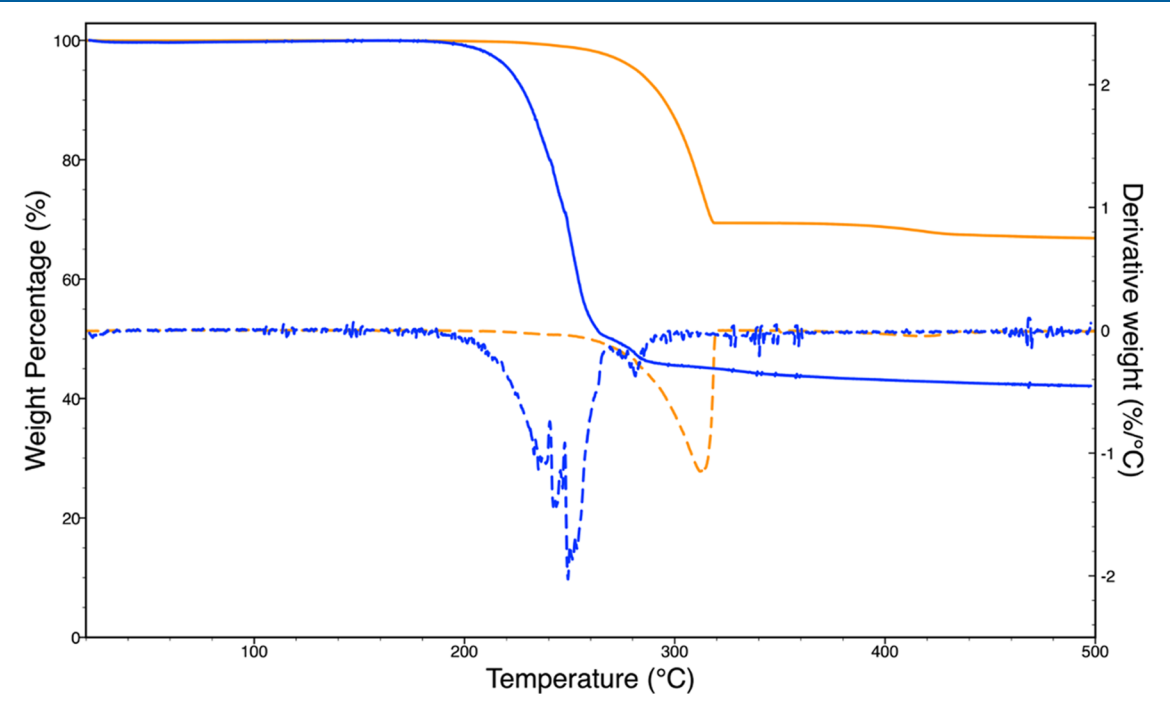


Figure 8. TGA analyses: solid blue line represented SLUG-53; dashed blue line represented 1st derivative of SLUG-53 trace; solid orange line represented SLUG-54; dashed orange line represented 1st derivative of SLUG-54 trace.

Langmuir model (Figure 5 and Table S7), and the maximum adsorption capacity was calculated to be 764 mg/g. This value is

very close to the theoretical maximum adsorption (770 mg/g) calculated by assuming 1 mol of SLUG-53 could uptake 1 mol of

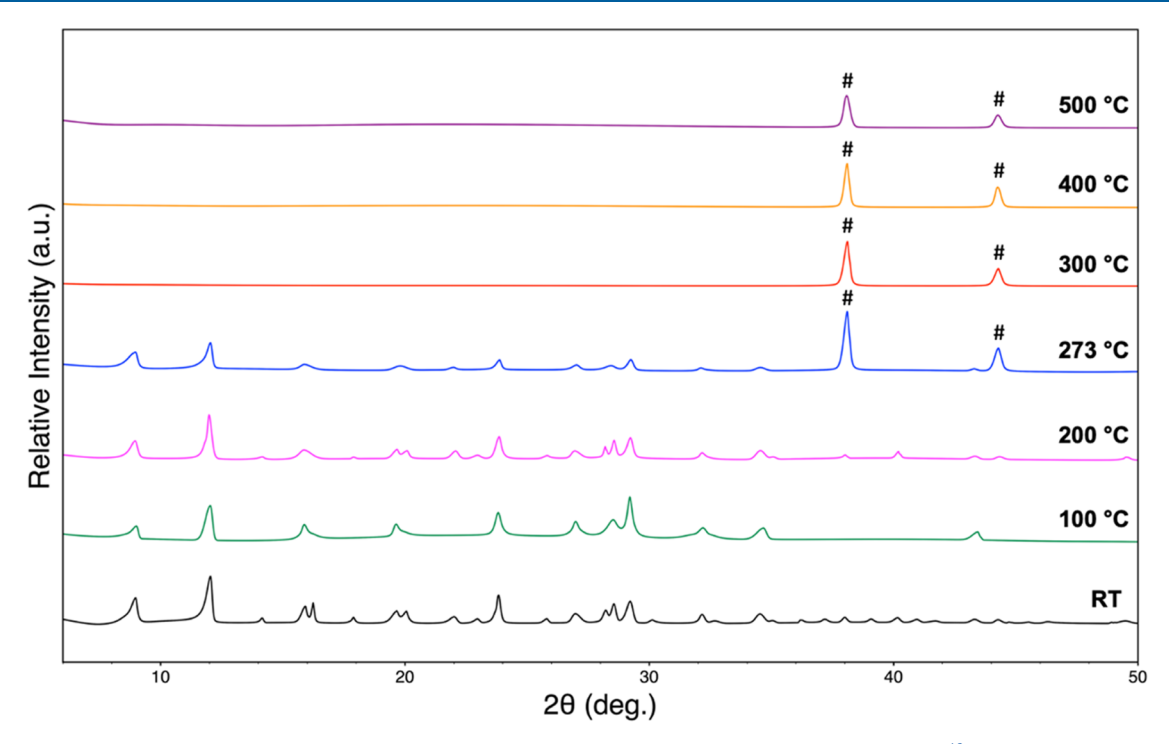


Figure 9. Ex situ VT-PXRD of SLUG-53. #: silver metal, Crystallographic Open Database (COD ID: 9012961). 40

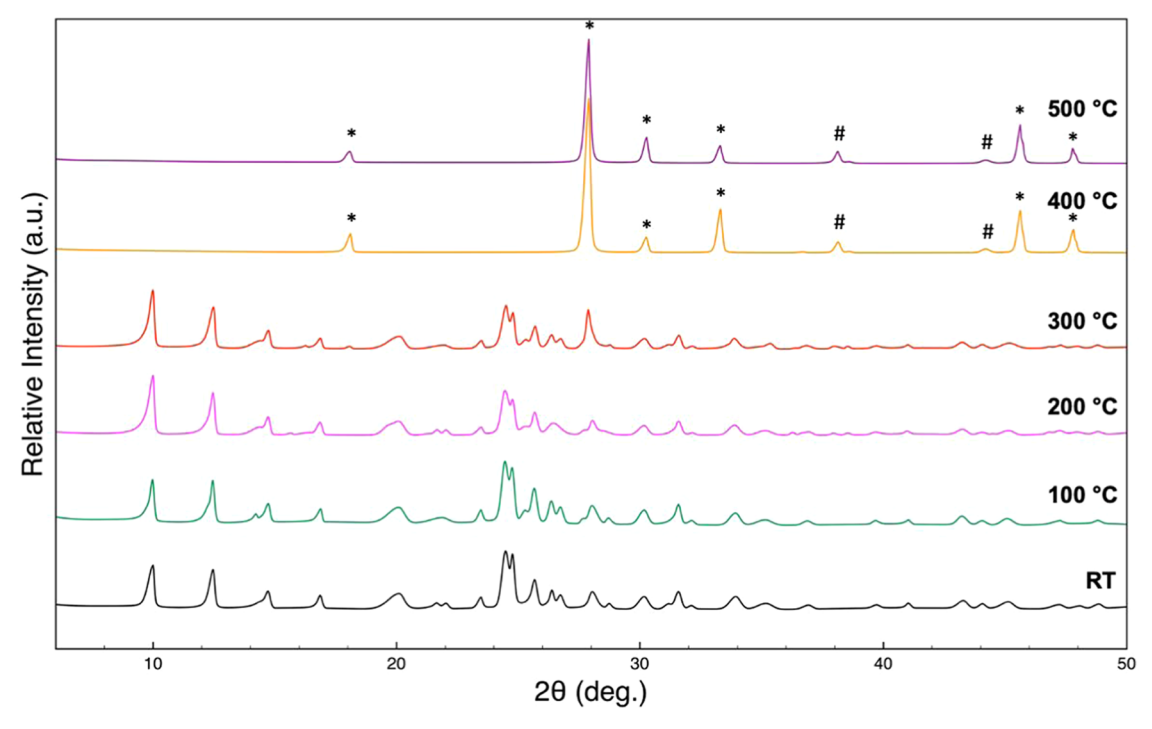


Figure 10. Ex situ VT-PXRD of SLUG-54. #: silver metal, COD ID: 9012961; 40 \*: silver perrhenate, COD ID: 2008824. 41

perrhenate. Although the adsorption capacity toward perrhenate is still lower than some commercial resins, <sup>34</sup> that of SLUG-53 is incredibly high and superior to most of the CP/MOF materials reported to date (Table S8). The data was also tested in the Freundlich model but showed significantly poorer fitting ( $R^2 = 0.644$ ) when compared to the Langmuir model ( $R^2 = 0.987$ ).

Sulfate ions may be present in great amounts in pertechnetate-containing waste. Because of the charge density,  $SO_4^{2-}$  has been shown to be more favorably adsorbed by other materials designed for the removal of the  $TcO^{4-}$ . SLUG-53, however,

retains excellent selectivity to adsorbing perrhenate in the presence of a molar excess of sulfate up to 200-fold (Table S9 and Figure S12).

Nitrate also presents a higher charge density than perrhenate. Its addition in excess to our systems led to interesting results. The perrhenate uptake increased in some of the conditions, when compared to systems not having nitrate (Figure S13). These results further show that SLUG-53 is a good candidate to be used in pertechnetate contaminated waste. It has been shown that anion-exchange reactions for materials composed of 4,4'-

bipyridine and  $Ag^+$  is ruled in part by the solubility of the original and the exchanged coordination polymers. Further investigation into solubility effects on the exchange behavior of 2,4′-bipirydine CPs is needed. Although not within the scope of this paper, it is an exciting topic for future studies.

The strong affinity SLUG-53 has shown for perrhenate, demonstrated by the high adsorption capacity values and selectivity studies, poses a challenge for its regeneration. Attempts to regenerate the starting materials by adding SLUG-54 to nitrate solution with large molar excesses (up to  $200 \times NO_3^-/SLUG-54$ ) at different temperatures (up to  $80\,^{\circ}C$ ) were unsuccessful.

**Exchange Mechanism Elucidation.** The mechanism by which ion exchange occurs in coordination polymers has long been discussed. Two main pathways are largely accepted in the field: single-crystal to single-crystal reactions (SCSC) and solvent-mediated recrystallization. 23 In order to further understand our system, the adsorption of perrhenate by SLUG-53 was monitored by SEM-EDS and PXRD. Figure 6 shows the rhenium SEM-EDS mapping for exchange reactions versus time using SLUG-53 single crystals as the starting material. Rhenium rich small crystals—as evidenced by PXRD to be SLUG-54 can be seen forming on the surface of the SLUG-53 large crystals. These results suggest a classic solvent-mediated recrystallization, where the new phase SLUG-54 is formed as perrhenate ions are fed to the original SLUG-53 from the surrounding solution. Furthermore, we hypothesize that imperfections in the starting crystals aid the new phase formation. We observed that in the case of a more regular and smoother surface, the majority of new phase growth occurred at the edges and fractures of the crystal (Figure 6).

The PXRD patterns in Figure 7 corroborate this mechanistic view. At shorter reaction times, there is a mix of SLUG-53/54 phases. As the reaction progresses, the SLUG-53 characteristic peaks are no longer observed. These results also agree with the ICP-OES analysis (Figure 4). At the end of the reaction (72 h), the measured adsorption was 97%, indicating the major species was indeed SLUG-54.

Because the perrhenate uptake reaction does not follow a SCSC mechanism, the flexible framework of SLUG-53 does not seem to play a major role in the perrhenate uptake. It may, however, be useful for other properties, particularly for sensing of gases or other guest ions from aqueous solutions.  $^{37-39}$ 

Thermostability Analysis. Thermogravimetric analysis shows that SLUG-54 is more stable than SLUG-53 (Figure 8), which would facilitate perrhenate abatement. For SLUG-53, one main event is observed at 215 °C and corresponds to the loss of 2,4'-bipyridine (mass loss observed: 49.13%; calculated: 47.90%). For SLUG-54, the same event is observed but at 295 °C (mass loss observed: 30.26%; calculated: 30.37%). As expected, no water loss peak was observed in the thermal profiles since there is no crystallographic water in the structures. The higher stability of the perrhenate CP can be hypothesized to be due to the eight-membered inorganic ring (Figure 3), which would more efficiently hold the framework together when compared to the soft argentophilic interactions of SLUG-53. The TGA results correlate well with VT-PXRD. For SLUG-53 (Figure 9), the usual powder pattern for the material is observed up to 200 °C. At 275 °C, there is a mixture of SLUG-53 and silver metal phase. Finally, only silver metal peaks are observed at 300 °C and above. For SLUG-54, the pure CP phase is observed until 300 °C (Figure 10). Starting at 400 °C, a mixture of silver metal and silver perrhenate phases is observed.

#### CONCLUSIONS

We presented two new  $[Ag(2,4'\text{-bipyridine})^+]$  CPs, both before and after exchange of the counteranion nitrate for perrhenate. The structural features of both materials allowed for the high-capacity sequestration of the incoming  $ReO_4^-$ . SLUG-53 is thus a promising material to be applied in the remediation of the perrhenate analogue pertechnetate. Our materials were all obtained and crystallized in aqueous media, avoiding the use of organic solvents. The elucidation of the recrystallization mechanism may aid the investigation of Ag(I) and 2,4'-bipy systems for the adsorption of other anions of interest. The thermal flexibility of SLUG-53 may lead to additional interesting properties such as the sensing of adsorbed molecules.

## ASSOCIATED CONTENT

# Supporting Information

The Supporting Information is available free of charge at https://pubs.acs.org/doi/10.1021/acs.inorgchem.4c00202.

Additional data and information: crystallographic tables, optical micrographs, thermal ellipsoids figures, disordered crystal structure for SLUG-55, PXRD patterns, overlay views, UV—vis spectra of adsorption experiments, tabular data including statistical errors for adsorption and selectivity experiments, selectivity results and a table with current high-performance materials for perrhenate adsorption from the literature (PDF)

# **Accession Codes**

CCDC 2209880–2209882 and 2303030 contain the supplementary crystallographic data for this paper. These data can be obtained free of charge via <a href="www.ccdc.cam.ac.uk/data\_request/cif">www.ccdc.cam.ac.uk/data\_request/cif</a>, or by emailing <a href="mailto:data\_request@ccdc.cam.ac.uk">data\_request/cif</a>, or by emailing <a href="mailto:data\_request@ccdc.cam.ac.uk">data\_request/ccdc.cam.ac.uk</a>, or by contacting The Cambridge Crystallographic Data Centre, 12 Union Road, Cambridge CB2 1EZ, U.K.; fax: +44 1223 336033.

# AUTHOR INFORMATION

#### **Corresponding Author**

Scott R. J. Oliver — Department of Chemistry and Biochemistry, University of California, Santa Cruz, Santa Cruz, California 95064, United States; orcid.org/0000-0002-6160-1518; Email: soliver@ucsc.edu

# **Authors**

Beatriz Ehlke — Department of Chemistry and Biochemistry, University of California, Santa Cruz, Santa Cruz, California 95064, United States; occid.org/0000-0002-3973-1383

Cambell S. Conour — Department of Chemistry and Biochemistry, University of California, Santa Cruz, Santa Cruz, California 95064, United States; orcid.org/0000-0001-9170-6436

**Tyler J. Vandiver** – Department of Chemistry and Biochemistry, University of California, Santa Cruz, Santa Cruz, California 95064, United States

Kevin C. Lofgren — Department of Chemistry and Biochemistry, University of California, Santa Cruz, Santa Cruz, California 95064, United States; orcid.org/0009-0004-3145-5478

Jeremy L. Barnett – Department of Chemistry and Biochemistry, University of California, Santa Cruz, Santa Cruz, California 95064, United States

Eric W. Reinheimer — Rigaku Americas Corporation, The Woodlands, Texas 77381, United States

John S. Wenger – Department of Chemistry and Biochemistry, University of California, Santa Cruz, Santa Cruz, California 95064, United States

Complete contact information is available at: https://pubs.acs.org/10.1021/acs.inorgchem.4c00202

#### Notes

The authors declare no competing financial interest.

## ACKNOWLEDGMENTS

This work was supported in part by the National Science Foundation under grant No. 2044692. The single-crystal X-ray diffractometer housed in the UCSC X-ray Diffraction Facility was funded by NSF MRI grant 2018501. We acknowledge Professor Timothy C. Johnstone and Dr. Daniel G. Droege of the UC Santa Cruz Department of Chemistry & Biochemistry and the X-ray Facility for SCXRD data collection. We also thank Dr. Brian Dreyer from the UC Santa Cruz Plasma Analytical Laboratory, RRID:SCR\_021925, for help with elemental analyses.

#### REFERENCES

- (1) Icenhower, J. P.; Qafoku, N. P.; Zachara, J. M.; Martin, W. J. The Biogeochemistry of Technetium: A Review of the Behavior of an Artificial Element in the Natural Environment. *Am. J. Sci.* **2010**, *310* (8), 721–752.
- (2) Desmet, G.; Myttenaere, C. Technetium in the Environment; Springer Science & Business Media, 2012.
- (3) Buzetzky, D.; Kovács, E. M.; Nagy, M. N.; Kónya, J. Sorption of Pertechnetate Anion by Cation Modified Bentonites. *J. Radioanal. Nucl. Chem.* **2019**, 322 (3), 1771–1776.
- (4) Shu, X.; Xu, Y.; Liu, L.; Fan, Y.; Zhuang, X.; Huang, C.; Chen, S.; Zheng, C.; Jin, Y.; Xia, C. Synthesis of New Carbazole Derivative Extractants and Study on Extraction of Perrhenate/Pertechnetate. *Polyhedron* **2022**, *214*, No. 115641.
- (5) Zhao, R.; Chen, D.; Gao, N.; Yuan, L.; Hu, W.; Cui, F.; Tian, Y.; Shi, W.; Ma, S.; Zhu, G. Porous Cationic Electrospun Fibers with Sufficient Adsorption Sites for Effective and Continuous <sup>99</sup>TcO<sub>4</sub><sup>-</sup> Uptake. *Adv. Funct. Mater.* **2022**, 32 (26), No. 2200618, DOI: 10.1002/adfm.202200618.
- (6) Zhang, P.; Chen, Y.-Z.; Weng, H.-Q.; Guo, Z.-F.; Chen, J.-L.; Zhao, X.; Ye, G.-A.; Lin, M.-Z. Dication-Accelerated Anion Transport inside Micropores for the Rapid Decontamination of Pertechnetate. *Nucl. Sci. Technol.* **2022**, 33 (4), 42.
- (7) Bonnesen, P. V.; Brown, G. M.; Alexandratos, S. D.; Bavoux, L. B.; Presley, D. J.; Patel, V.; Ober, R.; Moyer, B. A. Development of Bifunctional Anion-Exchange Resins with Improved Selectivity and Sorptive Kinetics for Pertechnetate: Batch-Equilibrium Experiments. *Environ. Sci. Technol.* **2000**, *34* (17), 3761–3766.
- (8) Celik, A.; Li, D.; Quintero, M. A.; Taylor-Pashow, K. M. L.; Zhu, X.; Shakouri, M.; Roy, S. C.; Kanatzidis, M. G.; Arslan, Z.; Blanton, A.; Nie, J.; Ma, S.; Han, F. X.; Islam, S. M. Removal of  ${\rm CrO_4}^{2-}$ , a Nonradioactive Surrogate of  ${\rm ^{99}TcO_4}^-$ , Using LDH $-{\rm Mo_3}{\rm S_{13}}$  Nanosheets. *Environ. Sci. Technol.* **2022**, *56* (12), 8590-8598.
- (9) Li, J.; Dai, X.; Zhu, L.; Xu, C.; Zhang, D.; Silver, M. A.; Li, P.; Chen, L.; Li, Y.; Zuo, D.; Zhang, H.; Xiao, C.; Chen, J.; Diwu, J.; Farha, O. K.; Albrecht-Schmitt, T. E.; Chai, Z.; Wang, S. <sup>99</sup>TcO<sub>4</sub><sup>-</sup> Remediation by a Cationic Polymeric Network. *Nat. Commun.* **2018**, 9 (1), No. 3007.
- (10) Li, J.; Li, B.; Shen, N.; Chen, L.; Guo, Q.; Chen, L.; He, L.; Dai, X.; Chai, Z.; Wang, S. Task-Specific Tailored Cationic Polymeric Network with High Base-Resistance for Unprecedented <sup>99</sup>TcO<sub>4</sub><sup>-</sup> Cleanup from Alkaline Nuclear Waste. ACS Cent. Sci. **2021**, 7 (8), 1441–1450.
- (11) Li, J.; Chen, L.; Shen, N.; Xie, R.; Sheridan, M. V.; Chen, X.; Sheng, D.; Zhang, D.; Chai, Z.; Wang, S. Rational Design of a Cationic

- Polymer Network towards Record High Uptake of <sup>99</sup>TcO<sub>4</sub><sup>-</sup> in Nuclear Waste. Sci. China: Chem. **2021**, 64 (7), 1251–1260.
- (12) Boglaienko, D.; Levitskaia, T. G. The Abiotic Reductive Removal and Subsequent Incorporation of Tc(IV) into Iron Oxides: A Frontier Review. *Environ. Sci.: Nano* **2019**, *6* (12), 3492–3500.
- (13) Rapti, S.; Diamantis, S. A.; Dafnomili, A.; Pournara, A.; Skliri, E.; Armatas, G. S.; Tsipis, A. C.; Spanopoulos, I.; Malliakas, C. D.; Kanatzidis, M. G.; Plakatouras, J. C.; Noli, F.; Lazarides, T.; Manos, M. J. Exceptional TcO<sub>4</sub><sup>-</sup> Sorption Capacity and Highly Efficient ReO<sub>4</sub><sup>-</sup> Luminescence Sensing by Zr<sup>4+</sup> MOFs. *J. Mater. Chem. A* **2018**, *6* (42), 20813–20821.
- (14) Pournara, A. D.; Evangelou, D. A.; Roukounaki, C.; Andreou, E. K.; Armatas, G. S.; Lazarides, T.; Manos, M. J. Highly Efficient Sorption and Luminescence Sensing of Oxoanionic Species by 8-Connected Alkyl-Amino Functionalized Zr<sup>4+</sup> MOFs. *Dalton Trans.* **2022**, *51* (45), 17301–17309.
- (15) Zhu, L.; Xiao, C.; Dai, X.; Li, J.; Gui, D.; Sheng, D.; Chen, L.; Zhou, R.; Chai, Z.; Albrecht-Schmitt, T. E.; Wang, S. Exceptional Perrhenate/Pertechnetate Uptake and Subsequent Immobilization by a Low-Dimensional Cationic Coordination Polymer: Overcoming the Hofmeister Bias Selectivity. *Environ. Sci. Technol. Lett.* **2017**, *4* (7), 316–322.
- (16) Xiao, C.; Khayambashi, A.; Wang, S. Separation and Remediation of <sup>99</sup>TcO<sub>4</sub><sup>-</sup> from Aqueous Solutions. *Chem. Mater.* **2019**, *31* (11), 3863–3877.
- (17) Soe, E.; Ehlke, B.; Oliver, S. R. J. A Cationic Silver Pyrazine Coordination Polymer with High Capacity Anion Uptake from Water. *Environ. Sci. Technol.* **2019**, 53 (13), 7663–7672.
- (18) Citrak, S. C.; Bdeir, K.; Delgado-Cunningham, K.; Popple, D.; Oliver, S. R. J. Exchange Capability of Cationic Silver 4,4'-Bipyrdine Materials for Potential Water Remediation: Structure, Stability, and Anion Exchange Properties. *Inorg. Chem.* **2019**, *58* (11), 7189–7199.
- (19) Chatenever, A. R. K.; Abdollahian, Y.; Oliver, A. G.; Oliver, S. R. J. Three Neodymium-Based Cationic Layered Inorganic Materials Capable of Anion Exchange. *Inorg. Chim. Acta* **2019**, *498*, No. 119171.
- (20) Zhu, L.; Xiao, C.; Dai, X.; Li, J.; Gui, D.; Sheng, D.; Chen, L.; Zhou, R.; Chai, Z.; Albrecht-Schmitt, T. E.; Wang, S. Exceptional Perrhenate/Pertechnetate Uptake and Subsequent Immobilization by a Low-Dimensional Cationic Coordination Polymer: Overcoming the Hofmeister Bias Selectivity. *Environ. Sci. Technol. Lett.* **2017**, *4* (7), 316–322.
- (21) Sheng, D.; Zhu, L.; Xu, C.; Xiao, C.; Wang, Y.; Wang, Y.; Chen, L.; Diwu, J.; Chen, J.; Chai, Z.; Albrecht-Schmitt, T. E.; Wang, S. Efficient and Selective Uptake of TcO<sub>4</sub><sup>-</sup> by a Cationic Metal—Organic Framework Material with Open Ag<sup>+</sup> Sites. *Environ. Sci. Technol.* **2017**, *51* (6), 3471–3479.
- (22) Shao, Z.; Huang, C.; Wu, Q.; Zhao, Y.; Xu, W.; Liu, Y.; Dang, J.; Hou, H. Ion Exchange Collaborating Coordination Substitution: More Efficient Cr(VI) Removal Performance of a Water-Stable  $Cu^{II}$ -MOF Material. *J. Hazar. Mater.* **2019**, 378, No. 120719.
- (23) Khlobystov, A. N.; Champness, N. R.; Roberts, C. J.; Tendler, S. J. B.; Thompson, C.; Schröder, M. Anion Exchange in Co-Ordination Polymers: A Solid-State or a Solvent-Mediated Process? *CrystEng-Comm* **2002**, *4* (71), 426–431.
- (24) Cui, X.; Khlobystov, A. N.; Chen, X.; Marsh, D. H.; Blake, A. J.; Lewis, W.; Champness, N. R.; Roberts, C. J.; Schröder, M. Dynamic Equilibria in Solvent-Mediated Anion, Cation and Ligand Exchange in Transition-Metal Coordination Polymers: Solid-State Transfer or Recrystallisation? *Chem. Eur. J.* 2009, 15 (35), 8861–8873.
- (25) Tong, M.-L.; Chen, X.-M.; Ye, B.-H.; Ng, S. W. Helical Silver(I)—2,4′-Bipyridine Chains Organized into 2-D Networks by Metal—Counterion or Metal—Metal Bonding. Structures of [Ag(2,4'-Bipyridine)]X ( $X^- = NO_3^-$  or  $ClO_4^-$ ). *Inorg. Chem.* **1998**, 37 (20), 5278–5281.
- (26) CrysAlisPro. Rigaku Oxford Diffraction. Version 171.41.103a, 2021.
- (27) SCALE3 ABSPACK A Rigaku Oxford Diffraction Program for Absorption Corrections, Rigaku Oxford Diffraction, 2017.

- (28) Sheldrick, G. M. SHELXT Integrated Space-Group and Crystal-Structure Determination. *Acta Crystallogr., Sect. A: Found. Adv.* **2015**, 71 (1), 3–8.
- (29) Sheldrick, G. M. Crystal Structure Refinement with SHELXL. Acta Crystallogr., Sect. C: Struct. Chem. 2015, 71 (1), 3–8.
- (30) Dolomanov, O. V.; Bourhis, L. J.; Gildea, R. J.; Howard, J. A. K.; Puschmann, H. OLEX2: A Complete Structure Solution, Refinement and Analysis Program. *J. Appl. Crystallogr.* **2009**, 42 (2), 339–341.
- (31) Spek, A. L. Structure Validation in Chemical Crystallography. *Acta Crystallogr., Sect. D: Biol. Crystallogr.* **2009**, 65 (2), 148–155.
- (32) Schmidbaur, H.; Schier, A. Argentophilic Interactions. *Angew. Chem., Int. Ed.* **2015**, 54 (3), 746–784.
- (33) Macrae, C. F.; Sovago, I.; Cottrell, S. J.; Galek, P. T. A.; McCabe, P.; Pidcock, E.; Platings, M.; Shields, G. P.; Stevens, J. S.; Towler, M.; Wood, P. A. Mercury 4.0: From Visualization to Analysis, Design and Prediction. *J. Appl. Crystallogr.* **2020**, 53 (1), 226–235.
- (34) Li, J.; Zhu, L.; Xiao, C.; Chen, L.; Chai, Z.; Wang, S. Efficient Uptake of Perrhenate/Pertechnenate from Aqueous Solutions by the Bifunctional Anion-Exchange Resin. *Radiochim. Acta* **2018**, *106* (7), 581–591.
- (35) Ming, M.; Zhou, H.; Mao, Y.-N.; Li, H.-R.; Chen, J. Selective Perrhenate/Pertechnetate Removal by a MOF-Based Molecular Trap. *Dalton Trans.* **2022**, *51* (11), 4458–4465.
- (36) Wang, S.; Yu, P.; Purse, B. A.; Orta, M. J.; Diwu, J.; Casey, W. H.; Phillips, B. L.; Alekseev, E. V.; Depmeier, W.; Hobbs, D. T.; Albrecht-Schmitt, T. E. Selectivity, Kinetics, and Efficiency of Reversible Anion Exchange with TcO<sub>4</sub><sup>-</sup> in a Supertetrahedral Cationic Framework. *Adv. Funct. Mater.* **2012**, 22 (11), 2241–2250.
- (37) Horike, S.; Shimomura, S.; Kitagawa, S. Soft Porous Crystals. *Nat. Chem.* **2009**, *1* (9), 695–704.
- (38) Schneemann, A.; Bon, V.; Schwedler, I.; Senkovska, I.; Kaskel, S.; Fischer, R. A. Flexible Metal—Organic Frameworks. *Chem. Soc. Rev.* **2014**, 43 (16), 6062–6096.
- (39) Lin, R.-B.; Li, F.; Liu, S.-Y.; Qi, X.-L.; Zhang, J.-P.; Chen, X.-M. A Noble-Metal-Free Porous Coordination Framework with Exceptional Sensing Efficiency for Oxygen. *Angew. Chem., Int. Ed.* **2013**, *52* (50), 13429–13433.
- (40) Owen, E. A.; Yates, E. L. XLI. Precision Measurements of Crystal Parameters. London, Edinburgh, Dublin Philos. Mag. J. Sci. 1933, 15 (98), 472–488.
- (41) Naumov, D. Yu.; Virovets, A. V.; Korenev, S. V.; Gubanov, A. I. Silver Perrhenate, AgReO4. *Acta Crystallogr., Sect. C: Cryst. Struct. Commun.* **1999**, *55* (8), IUC9900097.